Journal of Vacuum Science & Technology B

Atomic Precision Imaging with an On-Chip STM Integrated into a Commercial UHV STM System

Afshin Alipour,[1] S. O. Reza Moheimani,[1, a)] James H. G. Owen,[2] Ehud Fuchs,[2] and John N. Randall[2]
[1)]*Erik Jonsson School of Engineering and Computer Science, The University of Texas at Dallas, Richardson, TX 75080, USA*
[2)]*Zyvex Labs LLC, 1301 N Plano Rd., Richardson, TX 75081, USA*

(Dated: 29 May 2021)

In this article, we replace the Z axis of the piezotube of a conventional Ultra-High-Vacuum (UHV) Scanning Tunneling Microscope (STM) with a one-degree-of-freedom Microelectromechanical-System (MEMS) nanopositioner. As a result, a hybrid system is realized in which motions in the XY plane are carried out by the piezotube while the MEMS device performs the Z-axis positioning with a smaller footprint and higher sensitivity. With the proposed system and a feedback loop, STM imaging is conducted on a H-passivated Si (100)-2×1 sample in UHV condition, demonstrating this on-chip STM is conducive to atomic precision scanning tunneling microscopy.

I. INTRODUCTION

The key components of the Scanning Tunneling Microscope (STM) have changed little since its invention in early 1980s[1]. A piezoelectric actuator (usually a piezotube) moves a metallic probe with an atomically sharp tip in X, Y and Z directions, and the tunnel current feedback loop is a simple PI controller. Consequently, despite the unprecedented opportunities that STM has presented, its limited throughput inhibits its widespread use beyond surface science, especially as a nanofabrication tool[2], where its throughput is many orders of magnitude slower than e-beam lithography.

The limited throughput of the STM is rooted in its slow scan speed and its single-tip scheme to both of which its piezotube is a key contributor. The piezotube exhibits low bandwidth in all directions due to its bulkiness, especially in the Z axis where it directly interacts with the sample surface features, and when combined with a tip assembly, it is limited to about $1\,kHz$[3,4]. Besides, the bulk of the piezotube has led almost all STM systems to consist of only one tip, further restricting the throughput.

Microfabrication offers a promising pathway to redesigning the STM's electromechanical apparatus. A miniaturized STM nanopositioner, if designed properly, can possess high bandwidth due to its small mass[5,6]. Parallel operation of multiple tips is feasible by operating these miniaturized devices in an array, thereby multiplying the throughput[7–9]. We previously reported a high-bandwidth one-Degree-of-Freedom (1-DOF) Microelectromechanical-System (MEMS) nanopositioner to replace the Z axis of a STM piezotube[5]. This MEMS device exhibits bandwidth of $10\,kHz$ and a comparable Range of Motion (ROM) to the STM peizotube along the Z axis, i.e. $2\,\mu m$. Building on our previous efforts, we have redesigned the MEMS device to be compatible with a commercial Ultra-High-Vacuum (UHV) STM system. We describe steps taken to integrate the MEMS device into the UHV STM system and conduct STM imaging on a H-passivated Si (100)-2×1 sample with the MEMS device performing the Z-axis motion. The experimental results of STM imaging are then presented, demonstrating MEMS-based scanning tunneling microscopy.

In the following sections, the MEMS device is first redesigned in Section II to fit the UHV STM system of interest. Then in Section III, a hybrid STM system is achieved by integrating the MEMS device into the UHV STM system. In this section, we also point out how the original STM system is modified to support the electrostatic actuation methodology of the MEMS. With the new hybrid system, STM imaging is conducted, and results are presented in Section IV. Finally, the article is concluded and future work is laid out in Section V.

II. MEMS NANOPOSITIONER

The new MEMS device is meant to be a drop-in replacement for the conventional STM tip. Therefore, it should fit the area provided by the tip holder and the carrier that transfers it into the UHV system. For the UHV STM system of interest, a ScientaOmicron UHV Variable-Temperature (VT) STM, this translates to an area of $6\,mm \times 4.5\,mm$. Our previous design[5] exhibited stiffness of $160\,Nm^{-1}$ in simulations. For the new MEMS device, we intend to increase the stiffness to further suppress any thermal noise effect on stability of the tunneling junction[10]. With these considerations and other design requirements described previously[5], we redesigned the device. The stiffness was raised to $300\,Nm^{-1}$, and the device dimensions were reduced to $6\,mm$ and $4.3\,mm$. Finite element analysis shows the first resonance mode is located at $13.9\,kHz$. Electromechanical simulations predict the shuttle beam will have a displacement of $2.2\,\mu m$ by applying $69.6\,V$ to electrostatic comb drives just before pull-in instability occurs. The MEMS device is then fabricated by following the process flow reported in our previous work[5]. In order to improve the tip sharpness, the inplane Pt tip is further sharpened by Field-Directed-Sputter-Sharpening (FDSS) [11]. This process reduces the tip apex radius from $20\,nm$ to $10\,nm$. Figure 1 shows the Scanning-Electron-Microscope (SEM) images of the final device.

The fabricated device was characterized with a Laser Doppler Vibrometer (LDV) (MSA-100-3D, Polytec). The

[a)]Corresponding author: reza.moheimani@utdallas.edu.

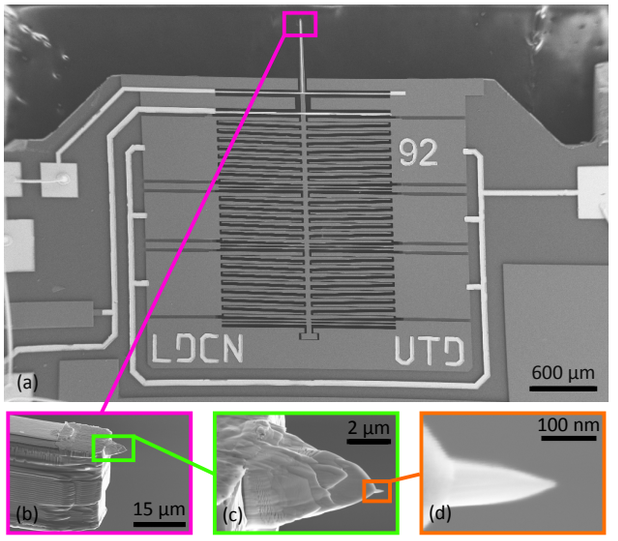

FIG. 1. SEM images of the Z-axis MEMS STM nanopositioner: (a) MEMS chip (b) shuttle beam end (c) in-plane Pt tip (d) tip apex.

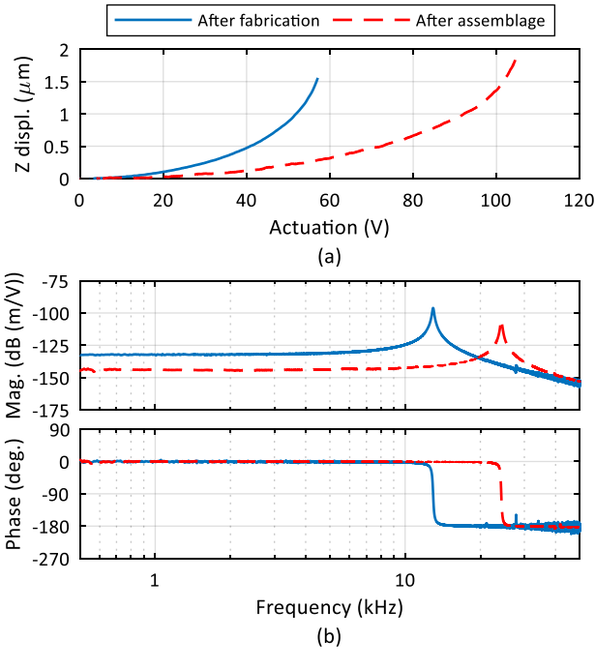

FIG. 2. Measured displacement of the MEMS device: (a) static response (b) frequency response with 20-V DC offset.

electromechanical static displacement was measured and is plotted in Fig. 2 a. We note that the device can reach 1.5-μm displacement when 57.1 V is applied to its actuators. Fig. 2 b illustrates the frequency response of the device along the Z axis. To obtain this measurement, a small-amplitude sinusoidal signal was superimposed on a 20-V offset and applied to the actuators. The harmonic displacement of the shuttle was then measured for the frequency range of interest. This figure reveals that the inplane resonance lies at 12.9 kHz.

III. HYBRID STM SYSTEM

The MEMS device is designed to be compatible with the ScientaOmicron UHV VT STM system. The base pressure of this system is 4×10^{-11} $Torr$. Thus, components introduced into the UHV system must not contain high-vapour-pressure materials. The standard system has a piezotube scanner with an XY range of 20 $\mu m \times 20$ μm, and a Z range of 1.3 μm. The maximum actuation voltage on the piezotube is ±135 V. The experiments reported here were conducted with the system's current preamplifier gain set to $3\,V/nA$, enabling current measurements up to 3.3 nA.

The sample used in the experiments is a $4\,mm\times10\,mm$ Si (100) prepared by 8-hr degassing, followed by flashing to 1240 $^\circ C$ three times, followed by H passivation from a hot W filament at a substrate temperature of 270 $^\circ C$, to give a well-passivated surface.

The STM is controlled by a STM control system (ZyVector, Zyvex Labs) running at 100-kHz sampling frequency, with four channels connected to the lateral electrodes of the piezotube, the inside electrode grounded, and the MEMS Z actuation signal delivered from the fifth amplifier channel. This arrangement enables us to independently control the Z motion of the MEMS device as well as lateral displacements of the piezotube scanner. Furthermore, we can choose to operate in 'passive mode' where the Z-actuation signal is mixed in with the XY-actuation signals and the piezotube operates in all three dimensions. When we shift to 'active mode', the Z signal to the piezotube is set to zero, and instead the Z direction is controlled by the MEMS. Therefore, no modification of the VT STM is necessary.

The Omicron piezotube scanner provides three contacts to a golden tip holder, two signals and one ground (Fig. 3 a). One signal contact measures the tunnel current, while the other, originally designed to pick up the QPlus signal, is used here to provide the MEMS actuation voltage. The MEMS device is attached onto the Omicron tip holder using UHV-compatible conductive silver epoxy (H20E, Epoxy Technology) (Fig. 3 c). Signal wires for the MEMS ground, tunnel current, and MEMS actuation are first wire-bonded on the MEMS device pads and then connected using the epoxy to the pins on the Omicron tip holder. The epoxied assembled device is then cured in an oven at a dwell time of 150 $^\circ C$ for one hour with a ramp up and down time of 1-3 $^\circ C$ per minute. The assembled Omicron tip holder and MEMS device are always checked for shorts prior and after assembly.

Frequency response of the MEMS shuttle was measured again with LDV after assembly and plotted in Fig. 2. Based on the measurements, we need to apply 102.2 V to the same device in order to reach the previous static displacement of 1.5-μm (Fig. 2 a). Moreover, the resonance frequency has increased to 24.2 kHz (Fig. 2 b), almost double in value. The results reflect an increase in the stiffness of the device which can be explained by tensile stresses induced in its flexures during the thermal process in the oven.

In constant-current scanning tunneling microscopy, a feed-

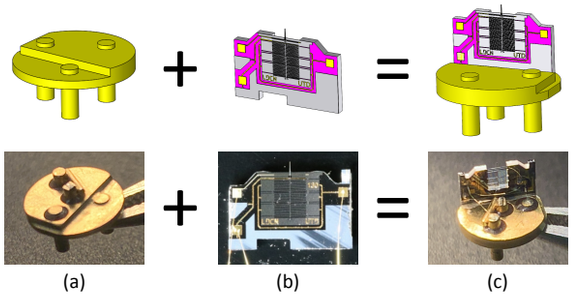

FIG. 3. Mounting the MEMS device on tip holder: (a) tip holder (b) MEMS device (c) MEMS assembly.

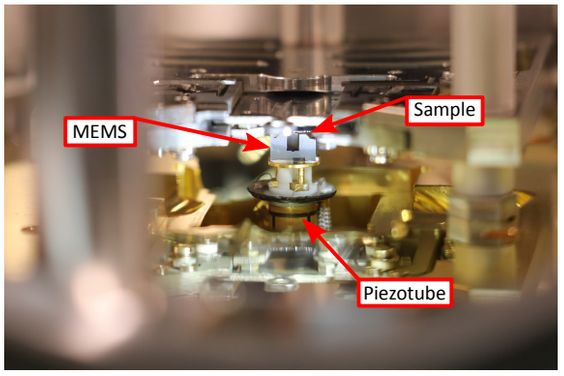

FIG. 4. The MEMS assembly mounted on the piezotube inside the ScientaOmicron UHV chamber.

back controller adjusts the tip height in order to maintain the tunneling current at a pre-specified setpoint. In this framework, variations in the tip-sample gap appear as disturbances entering the feedback loop that affect the measured tunneling current. The controller works to reject this disturbance, and the control command signal is interpreted as a measure of the sample surface topography. Here, the hybrid STM system utilizes the same feedback loop that is used for the Z axis of the piezotube of the original STM system. This feedback loop incorporates a proportional-integral controller. However, in order to eliminate the quadratic nature of the MEMS electrostatic actuation, the square root of the control command is used in the loop, as demonstrated in our previous work[5,6].

It is noteworthy to mention that the bias required for tunneling current establishment is applied to the tip, while the sample is kept at ground potential. The ground pin of the tip holder is also at the tip bias potential. As a result, there would be an offset equal to the bias on the ground plates of the parallel plate actuators. To remedy this issue, the ZyVector is programmed to superimpose the same offset on the counterplates, restoring the net actuation potential on the MEMS actuators.

IV. RESULTS

After successfully introducing the MEMS assembly to the UHV system and mounting it on the piezotube (Fig. 4), the Omicron's coarse piezomotors are used to position the piezotube so that the MEMS tip is close to the surface. An automated approach routine then moves the MEMS device closer to the sample surface such that it gets within ROM of the MEMS shuttle. In this procedure, the MEMS shuttle is extended fully with the feedback loop operative. If the surface is not detected, the shuttle is retracted, and the coarse motion takes one step towards the surface. This process is repeated until the MEMS motion detects the surface. With this method, we were able to establish stable tunneling current with multiple MEMS devices without crashing the MEMS tip into the sample. This process can be performed in either passive or active mode.

After establishing tunneling current with the hybrid system, the tip is raster scanned over the sample surface with the feedback loop regulating the tip-sample gap. Then an image is constructed by plotting the control command signal over the XY plane at a resolution of 512×256 pixels. Figures 5 (a)-(c) presents three STM images obtained with three different MEMS devices (Fig. 5 (d)-(f), respectively). For these experiments, the tunnel current setpoint was set to $0.5\,nA$ with the tip biased at $2.25\,V$ with respect to the sample. The tip speed was chosen to be $150\,nm/s$ in order to be comparable with the original STM system.

We observe that with the first two MEMS devices, the STM images are comparable in quality to those taken by standard W tips in commercial STMs. Figs. 5 (a) and (b) show H-terminated Si (100)-2×1 surfaces with single atomic steps 1.3-Å-high stepping down/up from the top-left/lower-right corner, respectively. The dimer rows of the Si (100)-2×1 reconstruction running in two perpendicular directions on alternate terraces are well-defined. Within the terraces, some white dots caused by missing H atoms and black holes caused by missing Si atoms are also visible. The MEMS device is therefore effective in controlling the Z position of the hybrid STM system and producing high-quality STM images.

The quality of the image produced by the third device shown in Fig. 5 (c), however, is visibly less than the other two. Although the terraces are visible with sharp edges, the dimer rows are only visible in one direction. This defect, which occurred in almost half of our initial trials, can be explained in terms of the tunneling phenomenon that the most prominent atom on the tip's apex makes the major contribution to the tunnel current. Due to over-etching of this tip during FDSS sharpening process, its geometry may have changed dramatically resulting in two adjacent Pt atoms at the top of the tip aligning with one of the dimer rows. As a result, this 'wedge' tip produces a double image which blurs out the dimer rows in one direction, but not the other, demonstrating that the geometry of the tip is a major determinant of the STM image quality. This speculation is further supported by SEM images of the tips which showed that there indeed exists a vertical wedge in some of the defective Pt tips in the same direction as the vertical dimers of the sample.

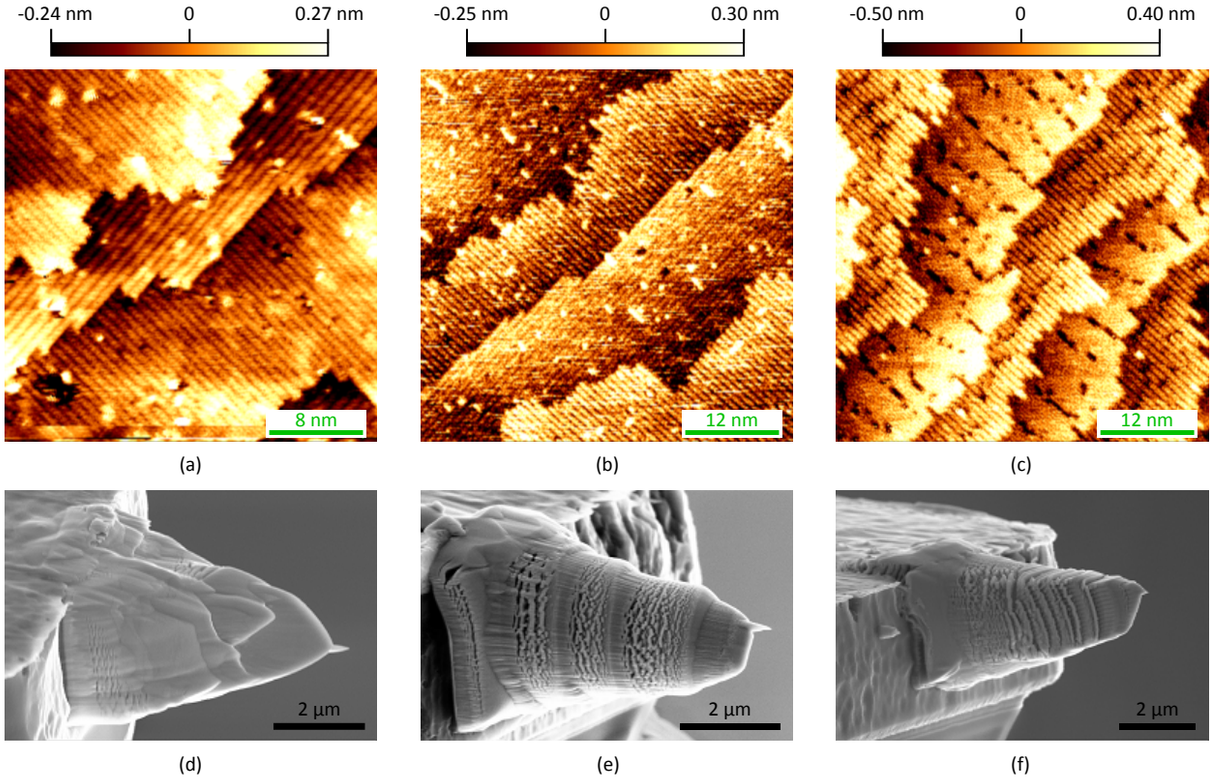

FIG. 5. STM imaging with the MEMS-based STM system with three different MEMS devices: (a)-(c) STM images, (d)-(f) respectively SEM images of the MEMS tips.

V. CONCLUSION

In this paper, we have reported STM imaging with a MEMS-based STM system. We redesigned a previously introduced high-bandwidth 1-DOF MEMS nanopositioner, and integrated it into a commercial UHV STM system. In the resulting system, the Z-axis motion is performed by the MEMS device, while the STM's piezotube scanner conducts lateral motions required for raster scanning of the sample in the XY plane. With the proposed system, STM imaging was successfully demonstrated on a H-passivated Si (100)-2×1 sample on a par with conventional STM systems, proving that proposed MEMS-based STM is conducive to atomic precision scanning tunneling microscopy.

Thanks to the MEMS device, the hybrid system possesses an order of magnitude higher bandwidth along Z axis compared to the original STM system, while maintaining the same ROM. In future work, we will take advantage of this increase in the bandwidth and demonstrate high-speed STM imaging with the hybrid system. This will involve performing closed-loop system identification experiments to estimate the Z-axis dynamics of the hybrid system[3,4], which is different from the piezotube-based system, and then synthesizing a controller to ensure satisfactory performance during high-speed scanning.

The small footprint of the MEMS nanopositioner presents a great opportunity for parallel scanning tunneling microscopy in which a number of closely placed 1-DOF MEMS nanopositioners are engaged with the sample surface at the same time, multiplying the STM throughput. Eventually, we aim to develop a parallel STM platform by using an array of Z-axis MEMS STM nanopositioners in future work.

VI. ACKNOWLEDGMENTS

This material is based upon work supported by the U.S. Department of Energy's Office of Energy Efficiency and Renewable Energy (EERE) under the Advanced Manufacturing Office Award No. DEEE0008322. Facilities provided by the University of Texas at Dallas Cleanroom Research Laboratory were used to fabricate this device. The authors wish to thank Zyvex Labs members, William R. Owen and Robin Santini for their assistance in setting up the experimental testbeds, and Rahul Saini for fruitful discussions.

VII. DATA AVAILABILITY

The data that supports the findings of this study are available within the article.

[1]G. Binnig and H. Rohrer, "Scanning tunneling microscopy," Surface Science **126**, 236–244 (1983).

[2]J. N. Randall, J. H. G. Owen, J. Lake, and E. Fuchs, "Next generation of extreme-resolution electron beam lithography," Journal of Vacuum Science & Technology B **37**, 061605 (2019).
[3]F. Tajaddodianfar, S. O. R. Moheimani, J. H. G. Owen, and J. N. Randall, "On the effect of local barrier height in scanning tunneling microscopy: Measurement methods and control implications," Review of Scientific Instruments **89**, 013701 (2018).
[4]F. Tajaddodianfar, S. O. R. Moheimani, and J. N. Randall, "Scanning tunneling microscope control: A self-tuning pi controller based on online local barrier height estimation," IEEE Transactions on Control Systems Technology **27**, 2004–2015 (2019).
[5]A. Alipour, M. B. Coskun, and S. O. R. Moheimani, "A high bandwidth microelectromechanical system-based nanopositioner for scanning tunneling microscopy," Review of Scientific Instruments **90**, 073706 (2019).
[6]A. Alipour, M. B. Coskun, and S. O. R. Moheimani, "A mems nanopositioner with integrated tip for scanning tunneling microscopy," Journal of Microelectromechanical Systems **30**, 271–280 (2021).
[7]J. N. Randall, J. H. G. Owen, J. Lake, R. Saini, E. Fuchs, M. Mahdavi, S. O. R. Moheimani, and B. C. Schaefer, "Highly parallel scanning tunneling microscope based hydrogen depassivation lithography," Journal of Vacuum Science & Technology B **36**, 06JL05 (2018).
[8]M. B. Coskun, M. Baan, A. Alipour, and S. O. R. Moheimani, "Design, fabrication, and characterization of a piezoelectric afm cantilever array," in *2019 IEEE Conference on Control Technology and Applications (CCTA)* (2019) pp. 227–232.
[9]M. Soleymaniha, M. B. Coskun, H. Mahmoodi Nasrabadi, A. Alipour, and S. O. R. Moheimani, "Design, fabrication and characterization of active atomic force microscope cantilever arrays," in *2021 IEEE 34th International Conference on Micro Electro Mechanical Systems (MEMS)* (2021) pp. 883–886.
[10]P. R. Saulson, "Thermal noise in mechanical experiments," Phys. Rev. D **42**, 2437–2445 (1990).
[11]S. W. Schmucker, N. Kumar, J. R. Abelson, S. R. Daly, G. S. Girolami, M. R. Bischof, D. L. Jaeger, R. F. Reidy, B. P. Gorman, J. Alexander, *et al.*, "Field-directed sputter sharpening for tailored probe materials and atomic-scale lithography," Nature communications **3**, 1–8 (2012).

VIII. FIGURE CAPTIONS

1. SEM images of the Z-axis MEMS STM nanopositioner: (a) MEMS chip (b) shuttle beam end (c) in-plane Pt tip (d) tip apex.

2. Measured displacement of the MEMS device: (a) static response (b) frequency response with 20-V DC offset.

3. Mounting the MEMS device on tip holder: (a) tip holder (b) MEMS device (c) MEMS assembly.

4. The MEMS assembly mounted on the piezotube inside the ScientaOmicron UHV chamber.

5. STM imaging with the MEMS-based STM system with three different MEMS devices: (a)-(c) STM images, (d)-(f) respectively SEM images of the MEMS tips.

Journal of Vacuum Science Technology B

PLEASE CITE THIS ARTICLE AS DOI: 10.1116/6.0001107

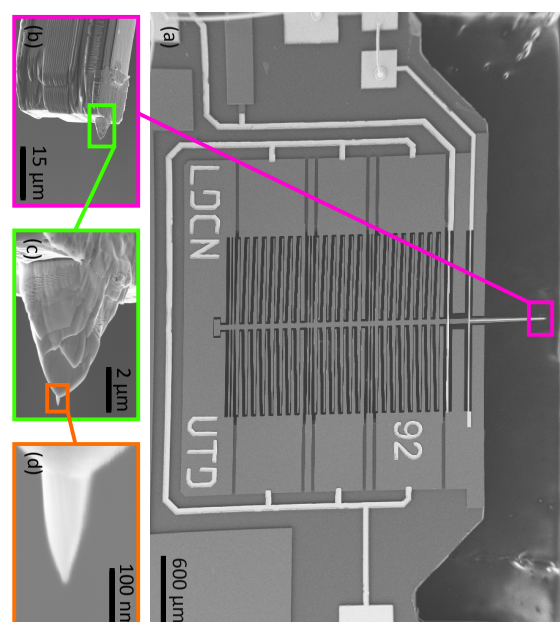

Journal of Vacuum Science Technology B

PLEASE CITE THIS ARTICLE AS DOI: 10.1116/6.0001107

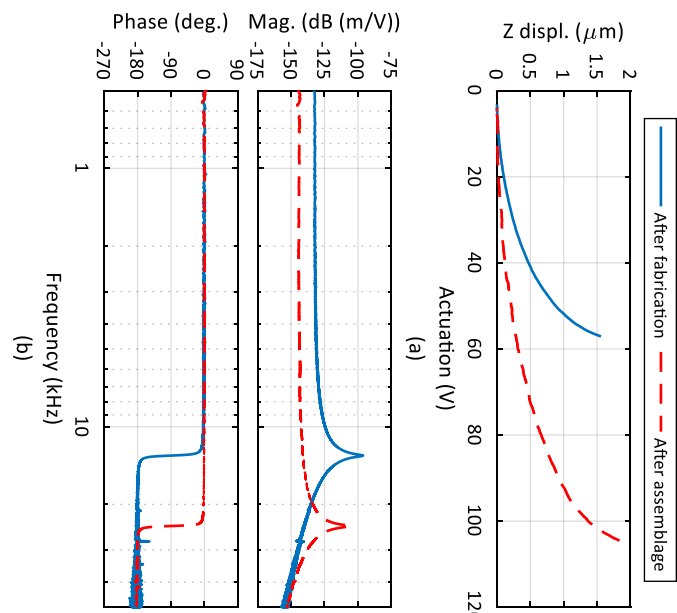

Journal of Vacuum Science Technology B

PLEASE CITE THIS ARTICLE AS DOI: 10.1116/6.0001107

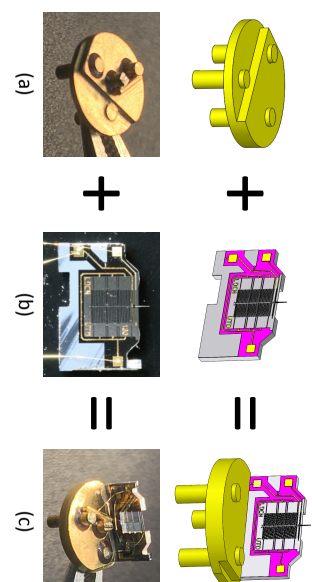

Journal of Vacuum Science Technology B

PLEASE CITE THIS ARTICLE AS DOI: 10.1116/6.0001107

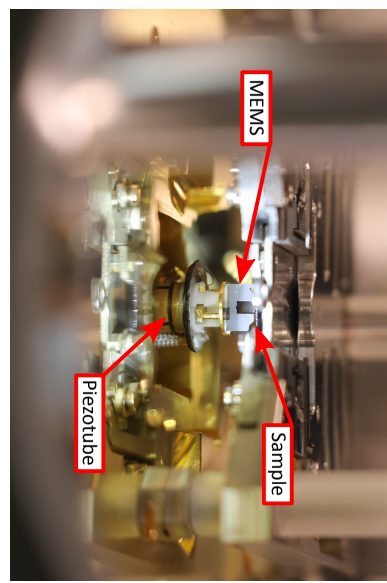

Journal of Vacuum Science Technology B